International Journal of Impact Engineering 42 (2012) 66–79

Contents lists available at SciVerse ScienceDirect

International Journal of Impact Engineering

journal homepage: www.elsevier.com/locate/ijimpeng

Dynamic crushing of cellular materials: Continuum-based wave models for the transitional and shock modes

Zhijun Zheng [a], Yaodong Liu [a], Jilin Yu [a,*], Stephen R. Reid [b]

[a] CAS Key Laboratory of Mechanical Behavior and Design of Materials, University of Science and Technology of China, Hefei, Anhui 230026, PR China
[b] School of Engineering, Fraser Noble Building, King's College, University of Aberdeen, Aberdeen AB24 3UE, UK

ARTICLE INFO

Article history:
Received 4 February 2011
Received in revised form
23 September 2011
Accepted 27 September 2011
Available online 4 October 2011

Keywords:
Cellular materials
Impact loading
Stress wave theory
Shock front
Transitional mode behaviour

ABSTRACT

As shown in the extensive studies of the dynamic responses of cellular materials, when the impact velocity is high, 'shock' waves can be generated. Because of the nature of the cellular structure, behind the 'shock (or compaction) front', there is a region of thickness approximately one single-cell-layer, across which the deformation can vary enormously, with strains of the order of ~0.8, say. This is due to the extensive and progressive crushing of the cells. The compressed part of the cellular material is *crushed* and *densified* as the material crosses the front. Depending on the details of the cellular geometry, this locally large deformation can be very intricate to model, however, a first order 'shock' model can be defined, which permits a useful understanding of the phenomenology of the dynamic deformation of cellular materials, particularly metal foams.

However, when the impact velocity is not very high, there exists a different type of front behind which the strain, though plastic, does not reach the densification strain. Based on one-dimensional continuum-based stress wave theory with a 'rigid unloading' assumption, in this paper a theoretical framework is established to explore the corresponding inherent mechanisms as a simple extension of the original 'shock' theory.

Two models, namely the Shock-Mode model and the Transitional-Mode model, are introduced. The distributions of stress, strain and velocity in the foam rod are derived. The theoretical results show that for a *Shock Mode*, behind the front the *initial* strain remains constant and the initial stress varies proportionally with the *square* of the impact velocity, but for a *Transition Mode*, the *initial* strain and stress behind the front reduce *linearly* with reducing impact velocity. The critical impact velocities for modes transition are predicted. Two dimensionless parameters, namely the *shock-enhancement* parameter and the *stress-hardening* parameter, are defined and the features of the theoretical predictions are presented. Compared to the experimental results, the responses at the ends of foam rod are well predicted by the present models and also by the R-P-P-L model. However, deformation mechanisms uncovered by the present modes and the R-P-P-L model are very different when the impact velocity is not very high.

The present simple, wave-based models extend the understanding of metallic foams to loading over a wider range of impact velocities than the previous models. In particular, the sub-shock-like behaviour, which has not yet been dealt within the literature, can be better understood through the new Transitional-Mode model.

1. Introduction

1.1. Dynamic crushing of cellular materials

Cellular materials combine light weight and high mechanical energy absorption capacity and are widely used in several engineering applications, especially in the automotive, aerospace and defence industries. As energy absorbers for impact and blast protection, their responses to dynamic loading have attracted considerable research interest. In the past decade, extensive experimental, numerical and theoretical studies have been conducted to investigate the dynamic behaviour of cellular materials, in particular metallic (aluminium) foams and honeycombs.

One common phenomenon is that, when a cellular material (say, wood [1], a 3D aluminium foam [2,3] or a 2D aluminium honeycomb [4,5]) is subjected to high velocity compressive impact

* Corresponding author. Tel.: +86 551 360 0792; fax: +86 551 360 6459.
E-mail address: jlyu@ustc.edu.cn (J. Yu).

0734-743X/$ – see front matter © 2011 Elsevier Ltd. All rights reserved.
doi:10.1016/j.ijimpeng.2011.09.009

(discussed in Section 2), cells near the impact end collapse layer-by-layer and a deformation front results. Because of the nature of the cellular structure, the front is located at a narrow region of approximately the width of a single-cell-layer [6], across which the deformation can vary significantly, with strains of the order of ~0.8, say. This is due to the extensive and progressive crushing of the cells. It is difficult to describe accurately the variations in the physical quantities at the meso/micro-scale because the response of the cell geometry could be complex, undergoing locally large mesoscopic deformation and large local microscopic displacements at the intercellular scale, some of this unstable.

Even so, when the material is viewed as a continuum and the basic conservation laws of mass and momentum are invoked, concepts from continuum wave theory may be used. These result in a relatively simple mathematical model which has been shown through comparison with the experimental results to be valid at a first order level [1–3]. The physical quantities such as the stress, strain and velocity should be defined in a macroscopic perspective, which requires the statistical average is measured over the range of a few cell sizes. For impact loading, these models were based on elements of 'shock theory' where a macroscopic discontinuity in the physical quantities gave a good representation of the physical behaviour. This phenomenon is therefore often termed a 'shock (or compaction) front' as described in Refs. [1–3].

In this case, the cell size is an intrinsic length scale which can be used in 2D models to define parameters such as 'strain' (for a 2D illustration, see [7]). The width of the shock is of the order of the cell size. Behind the shock front, the material is *crushed* and *densified* (i.e. its strain is raised to the densification strain, as defined below). A typical 3D distribution of cell deformation in an aluminium foam is shown in Fig. 1a and the corresponding deformation mode was referred as of the 'shock' type by Tan et al. [2] and is qualitatively the same as that predicted in 2D honeycomb models. This deformation mode was also referred to the '*I*'-shaped pattern by Ruan et al. [4], the Dynamic mode by Zheng et al. [5], the *Shock Mode* (used hereafter) by Liu et al. [6] or the progressive mode by Ma et al. [8] when describing the behaviour during the in-plane crushing of 2D aluminium honeycombs based on cell-based finite element models (FEM). The use of FEM for 2D models has enabled more details of the meso-scale deformation of the cellular structure of the foam to be modelled. When a specimen is subjected to a dynamic compressive loading, different responses at its two ends have been observed, with shock-enhancement dominating the behaviour at the proximal end [6–9]. Inertia has significant influence on the dynamic response of cellular materials [10].

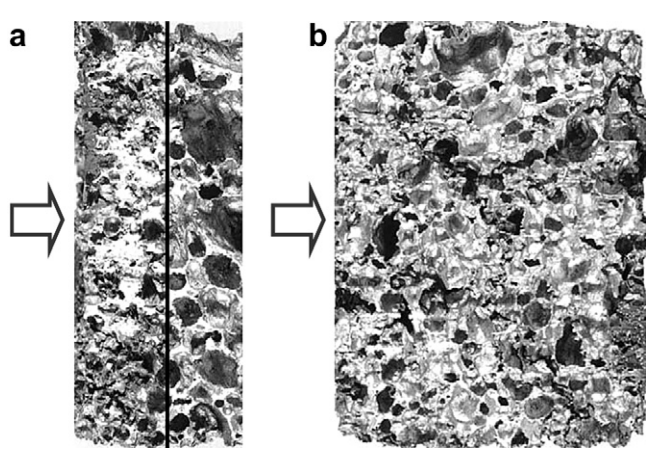

Fig. 1. Typical distributions of cell deformation for the initial impact velocities of (a) $V_0 = 107.5$ m/s and (b) $V_0 = 22.4$ m/s, respectively [2].

However another common phenomenon, evident in both the 2D honeycomb models [4–7] and the 3D experimental observations [2], is that, when the impact velocity is *not* very high (although generating inelastic behaviour) there exists a different type of deformation front behind which the strain, though plastic, does not reach the densification strain as described in Ref. [6]. In this case, a '*V*'-shaped pattern of deformation was predicted in the in-plane crushing of regular hexagonal honeycombs [4]. However, a different pattern of deformation referred as the *Transitional Mode* was predicted in irregular honeycombs [5], i.e. the deformation is mesoscopically uneven but the wave front is macroscopically flat. The two patterns of deformation are caused by the effects of inertia, the boundary constraints as well as weak shear bands to some extent. Weak shear bands are typical in cellular solids and are usually short and randomly located in an irregular honeycomb under compression, but in a regular honeycomb there also exist weak shear bands in a certain loading directions [11]. This leads to the difference in the two patterns.

Turning to the 3D case, commercial aluminium foam has cell irregularity and so its deformation at a moderate impact velocity is most likely similar with that of irregular honeycombs. Limited to the 3D experimental conditions, it is difficult to observe the full deformation process or obtain the distribution of "macroscopic" strain/stress in a real specimen. Experimental researches in the literature, for example [2], only presented the final stage of the crushing. Fig. 1b for a Hydro/Cymat aluminium foam taken from Fig. 13b of Ref. [2] presents a typical distribution of cell deformation of 3D aluminium foam at a moderate impact velocity, which may result from the deformation process in Transitional Mode. The strain distribution from 3D cell-based finite element models may help to provide more clear evidence, but such models are not yet available. In Ref. [2] the terms super-critical and sub-critical (impact) velocities were used to distinguish the different response modes. In this paper, the distinction between the two types of behaviour is termed Shock and Transitional Modes. This reflects the more detailed description that is possible when dealing with foams having a more regular structure such as Duocel foam [12].

1.2. Origins of the simple 'shock' models

Deformation front localisation and stress/strain non-uniformity in the dynamic crushing of cellular materials are related to the propagation of plastic shock or wave fronts. The idea of 'structural shock' propagation to model the 'discontinuous' behaviour was first used by Reid et al. [13]based on experiments on a one-dimensional discrete ring system. Several methods have been proposed to model the 'shock' propagation in cellular materials, which are summarized as follows.

A one-dimensional spring-mass model was presented by Shim et al. [14]for modelling impact deformation of open-cell structures in which an individual cell is strain-softening. The spring-mass model was further developed by Li and Meng [15]to study the attenuation or enhancement in cellular material. However recently, Harrigan et al. [16]have argued that mass-spring models are not capable of modelling the discontinuities that exist in a compaction wave in cellular materials.

A simple rate-independent, rigid–perfectly plastic–locking (R-P-P-L) shock model was first developed by Reid and Peng [1] to explain experimental results showing an enhancement of the crushing strength of wood specimens. They found the predictions using this theory compared well with experimental stresses associated with the propagation of the crushing process. This model was further extended to metallic foams by Tan et al. [3] to estimate the magnitude of the shock-induced stress enhancement. Two different impact scenarios were analyzed by these authors [3] using

a thermo-mechanical approach to achieve a first order understanding of the dynamic compaction process.

An elastic–perfectly plastic–rigid (E-P-P-R) model was proposed by Lopatnikov et al. [17] to consider the elastic effect and further discussed by Li and Reid [18]to clarify the shock wave propagation in cellular materials. In these shock wave modes, the shock-like deformation was considered to occur when a locking (densification) strain is attained and so the models should only be applied to those states corresponding to the *Shock Mode*. A more realistic constitutive relationship for cellular materials (wood loaded along the grain) was used by Harrigan et al. [19]to achieve a more accurate model. The R-P-P-L shock model was extended by Pattofatto et al. [20]for a power-law hardening locking to understand the behaviour of shock-enhancement, but only a constant impact velocity was considered, i.e. the effect of finite striker mass was ignored.

1.3. Outline of this paper

In order to extend the understanding of metallic foams to loading at different impact velocities, simple, wave-based models for the *Transitional Mode* and the *Shock Mode* are investigated in this paper. The assumptions for the theoretical models are introduced in Section 2 and the theoretical derivations are presented in Section 3. Comparisons and discussions are carried out in Section 4, followed by conclusions in Section 5.

2. Continuum-based shock wave models and their assumptions

Two impact scenarios, as represented schematically in Fig. 2, are investigated in this study. One is that of a foam rod with a backing mass striking axially against a stationary target, abbreviated as *the rod-target impact*. The other is that of a rigid striker striking axially against a stationary foam rod, denoted as *the striker-rod impact*. The mass of the striker is M_b and its initial velocity is V_0. The length of the foam rod is l_0 and its density is ρ_0. Treating the rod as a continuum, it is assumed to be initially uniform and homogeneous, as in Tan et al. [3]. For simplicity, one-dimensional loading and 'rigid unloading' assumptions are employed in the continuum-based wave theory used in this paper. The practical foundation involved in these assumptions is discussed in Section 4.3.

On the basis of experimental studies, the quasi-static, compressive behaviour of a cellular material is often described by a global, characteristic, constitutive relationship between the nominal stress and the nominal strain based on the overall length of the specimen[1]. Following early elastic behaviour, the deformation passes through a yield point, followed by a plateau region over a large strain range, culminating in 'locking or densification' [1,2]. Although it has long been known that the quasi-static deformation mechanisms are non-uniform, consisting of local collapse in the cell structure, the 'extensive' load-deflection behaviour can be simply converted into 'intensive' stress-strain curves in an obvious manner (see simple argument on p. 536 of Ref. [1]). Interestingly, due to the localisation of deformation at or near to 'crush-fronts' due to inertia effects, the dynamic deformation becomes much dominated by the propagation of these fronts, see [2]. This behaviour enabled shock theory to be used to model high velocity crushing in aluminium foams [3]. This use of continuum wave theory provides a first order, simple, continuum mechanics basis for modelling the dynamic response of cellular materials. This paper is in the 'continuum spirit' of this type of modelling.

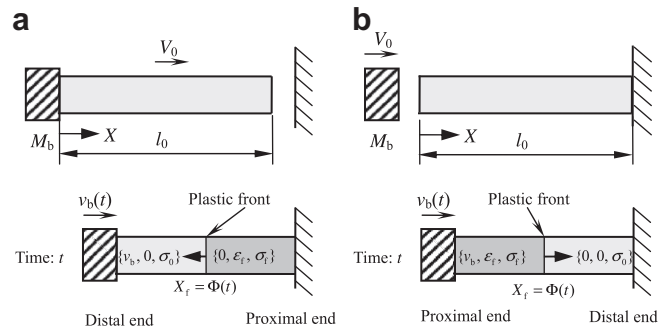

Fig. 2. Two impact scenarios: (a) the rod-target impact and (b) the striker-rod impact. The physical quantities behind or ahead of the front before reaching the distal end are labelled.

Three deformation modes were observed in the uniaxial dynamic crushing of 2D Voronoi honeycombs under different impact velocities, and the critical impact velocities for modes transition were evaluated [5,6]. The *Quasi-static 'Homogeneous' Mode* occurs under a *low* impact velocity. In this mode, the crush bands are randomly located, but the stresses at the proximal and distal ends are almost in equilibrium and so the stress field is viewed in a macroscopically homogeneous manner. At a *moderate* impact velocity, the *Transitional Mode* is evident. In this mode, the stress distribution is far from being in equilibrium, but the crush bands are initiated nearer to the proximal end than to the distal end. The strain does not reach the densification strain [6]. Moreover, the slope of the plateau zone in the nominal quasi-static stress-strain curve usually increases with increasing nominal strain. When the impact velocity is *high* enough, the *Shock Mode* occurs in which the cells are crushed sequentially, layer-by-layer from the proximal end. Meanwhile, the nominal strain in the crushed part of the cellular material reaches the densification strain ε_D. We denote the critical impact velocities for modes transition from the Homogenous Mode to the *Transitional Mode* and from the *Shock Mode* to the *Transitional Mode* as the first and second critical impact velocities, V_{c1} and V_{c2}, respectively.

Following the work of Avalle et al. for clarity of definition, the densification strain is usually defined as the strain corresponding to the maximum of the energy absorption efficiency [21,22,2]. However the uncertainty in the definition of ε_D is still a matter for debate [20], though this is not pursued here. As mentioned in Section 1, the deformation of irregular honeycombs is microscopically uneven but the deformation front is macroscopically flat. One-dimensional behaviour is therefore assumed here to model the deformation front propagating through an irregular honeycomb or foam.

A simple quasi-static compressive model for shock wave in cellular material was presented by Reid et al. [1,3] and it is called the R-P-P-L idealisation. In this model, there are only two material parameters used to define the material properties: the plateau stress σ_{pl} and the locking strain ε_L. The second parameter was taken to be the densification strain ε_D as defined above, as depicted in Fig. 3. The first parameter is defined as the average stress over the range of the yield strain ε_y to the densification strain ε_D. However to establish a model for the *Transitional Mode* as a simple extension of the original 'shock' theory and further improve the model for the deformation, here we employ a linearly hardening plastic stage in the quasi-static stress-strain relationship of cellular materials, i.e.

[1] Given the 3D cellular nature of foams, the notions of nominal stress and strain are arguable. However, a continuum framework is convenient for engineering design calculations and will be adopted herein for convenience, drawing particularly on the understanding gained for 2D systems derived from computational models for insight into the detailed deformation mechanisms.

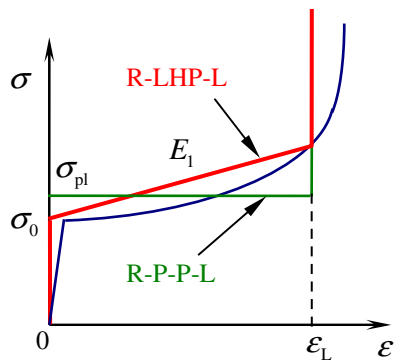

Fig. 3. Rigid–Perfectly Plastic–Locking (R-P-P-L) idealisation and Rigid–Linearly Hardening Plastic–locking (R-LHP-L) idealisation of the nominal quasi-static stress-strain curve of a cellular material.

using a rigid–linearly hardening plastic–locking (R-LHP-L) idealisation, as shown also in Fig. 3. In this idealisation, there are thus three material parameters: the yield stress σ_0, the hardening modulus E_1 and the locking strain ε_L. The hardening modulus E_1 is determined by the slope of the line linking the two stress-strain states of $(0, \sigma_0)$ and $(\varepsilon_D, \sigma_D)$, in which σ_D is the stress corresponding to the first attainment of the densification strain in the quasi-static stress-strain relationship. The R-LHP-L idealisation degenerates to the R-P-P-L idealisation when E_1 becomes zero. However, for real foams, the quasi-static stress-strain curves usually have a slow hardening plastic stage before densification, so E_1 is usually greater than 0.

When a foam rod modelled by the R-LHP-L idealisation is loaded by a suddenly applied pulse whose peak value is higher than the yield strength, an 'elastic' loading wave is generated first which, in this approximation, travels with an infinite speed along the rod followed by a plastic loading wave propagating behind this elastic loading wave. As the load is reduced, an elastic unloading wave follows the plastic loading wave. This situation is equivalent to a rigid striker impacting the proximal end of the rod at a sufficiently high impact velocity. Unloading occurs when the speed of the striker is reduced due to the stress in the material. Generally, the unloading elastic wave speed is larger than the plastic wave speed, so the elastic unloading wave catches up with the plastic loading wave. The two stress waves interact and the strength of the plastic loading wave is attenuated, finally becoming an elastic wave. In the present modelling, we regard the unloaded part of the rod to be rigid.

3. Theoretical derivations based on the stress wave theory

3.1. The rod-target impact scenario

3.1.1. Moderate velocity impact

3.1.1.1. The case before wave reflection. For a moderate velocity impact, the rod is deformed in the *Transitional Mode* during the propagation of the plastic wave front moving from the proximal end to the distal end. The part behind the front is stationary while the part ahead of the front moves together with the rigid mass. The physical quantities behind the front are $\{0, \varepsilon_f(t), \sigma_f(t)\}$ and those ahead of the front are $\{v_b(t), 0, \sigma_0\}$, where t is the time and $\{v, \varepsilon, \sigma\}$ denotes a list of the physical quantities including the velocity, strain and stress. Based on the inertial law, the acceleration of the mass can be calculated as

$$a_b(t) = \frac{-\sigma_0 A_0}{M_b + \rho_0 A_0 X_f} = -\frac{\sigma_0}{m + \rho_0 \Phi(t)}, \tag{1}$$

where $X_f = \Phi(t)$ is the position of the wave front. The above equation can also be obtained by applying the condition of momentum conservation of the system, see Appendix for the derivation. The area of the rod is A_0, which is considered as a constant during the crushing process, and $m = M_b/A_0$ is the specific mass of the rod per unit area.

According to the R-LHP-L idealisation, the Lagrangian velocity of the front is $\dot{\Phi}(t) = -C_1$ and the position of the front is $\Phi(t) = l_0 - C_1 t$, where the dot symbol (.) is used here for the derivative with respect to the time and $C_1 = \sqrt{E_1/\rho_0}$. Integrating the acceleration of the mass, we have its velocity

$$v_b(t) = V_0 + \int_0^t a_b(t)\mathrm{d}t = V_0 + C_1 \frac{\sigma_0}{E_1} \ln\left[1 - \frac{\rho_0 C_1 t}{m + \rho_0 l_0}\right]. \tag{2}$$

According to the stress wave theory [23], the kinematic compatibility condition across the front is written as

$$0 - v_b(t) = \dot{\Phi}(t)\left(\varepsilon_f(t) - 0\right) \tag{3}$$

and the kinetic compatibility condition across the front is given by

$$\sigma_f(t) - \sigma_0 = \rho_0 \dot{\Phi}(t)(0 - v_b(t)), \tag{4}$$

which are derived from the conservation conditions of mass and momentum across the front, respectively, see Appendix for the derivations. The conservation condition of energy across the front has not been used as a basic equation in this paper, because it is naturally satisfied when Eqs. (3) and (4) are used as the basic equations. A discussion on the basic equations has been carried out by Harrigan et al. [16]. From the above equations, we have the strain and stress behind the wave front

$$\varepsilon_f(t) = \frac{v_b(t)}{C_1} = \frac{V_0}{C_1} + \frac{\sigma_0}{E_1} \ln\left[1 - \frac{\rho_0 C_1 t}{m + \rho_0 l_0}\right] \tag{5}$$

and

$$\sigma_f(t) = \sigma_0 + \rho_0 V_0 C_1 + \sigma_0 \ln\left[1 - \frac{\rho_0 C_1 t}{m + \rho_0 l_0}\right], \tag{6}$$

respectively. From the two above equations, the *initial* strain and stress behind the wave front are found to be

$$\begin{cases} \varepsilon_f(0) = V_0/C_1 \\ \sigma_f(0) = \sigma_0 + \rho_0 V_0 C_1 \end{cases}, \tag{7}$$

which reduce *linearly* with reducing impact velocity in the *Transitional Mode*. The time when this front reaches the distal end is

$$t_1 = l_0/C_1, \tag{8}$$

which is determined from $\Phi(t_1) = l_0 - C_1 t_1 = 0$. The corresponding velocity of the mass is

$$v_b(t_1) = V_0 - C_1 \frac{\sigma_0}{E_1} \ln(1 + \mu), \tag{9}$$

where $\mu = \rho_0 l_0/m$. The plastic yield stress and strain at location X are

$$\sigma_p(X) = \sigma_f((l_0 - X)/C_1) = \sigma_0 + \rho_0 V_0 C_1 + \sigma_0 \ln \frac{m + \rho_0 X}{m + \rho_0 l_0} \tag{10}$$

and

$$\varepsilon_p(X) = \varepsilon_f((l_0 - X)/C_1) = \frac{V_0}{C_1} + \frac{\sigma_0}{E_1} \ln \frac{m + \rho_0 X}{m + \rho_0 l_0}, \tag{11}$$

respectively. So, the physical quantities in the rod at position X and time t are expressed as

$$\{\bar{v},\bar{\varepsilon},\bar{\sigma}\} = \begin{cases} \{v_b(t),0,\sigma_0\}, & 0 \le X < l_0 - C_1 t \\ \left\{0,\varepsilon_p(X),\sigma_f(t)\right\}, & l_0 - C_1 t < X \le l_0 \end{cases} \tag{12}$$

in which $v_b(t)$, $\varepsilon_p(t)$ and $\sigma_f(t)$ are presented in Eqs. (2), (11) and (10), respectively. We denote this model as the Transitional-Mode model.

3.1.1.2. The case after wave reflection. When the wave front reaches the distal end, a reflected wave will form and so a plastic wave (possibly shock) front will propagate from the distal end to the proximal end. If the rod deforms also in the *Transitional Mode* after wave reflection, we still can easily determine the wave velocity from the R-LHP-L idealisation. The Lagrangian velocity of the front is $\dot{\Phi}(t) = C_1$ and its location is $\Phi(t) = C_1(t-t_1)$. The physical quantities behind the front are $\{v_b(t), \varepsilon_f(t), \sigma_f(t)\}$ and those ahead of the front are $\{0, \varepsilon_p(\Phi(t)), \sigma_p(\Phi(t))\}$. From the R-LHP-L idealisation, the stress behind the front can be determined as

$$\sigma_f(t) = \sigma_p(\Phi(t)) + E_1\left(\varepsilon_f(t) - \varepsilon_p(\Phi(t))\right) = \sigma_0 + E_1\varepsilon_f(t), \tag{13}$$

and so the acceleration of the mass is

$$a_b(t) = -\frac{\sigma_f(t)A_0}{M + \rho_0 A_0 \Phi(t)} = -\frac{\sigma_0 + E_1\varepsilon_f(t)}{m + \rho_0 C_1(t-t_1)}. \tag{14}$$

Using the kinematic compatibility condition across the front

$$v_b(t) - 0 = \dot{\Phi}(t)\left(\varepsilon_f(t) - \varepsilon_p(\Phi(t))\right), \tag{15}$$

and the Lagrangian velocity of the front $\dot{\Phi}(t) = C_1$, we have the acceleration of the mass

$$a_b(t) = \dot{v}_b(t) = C_1\dot{\varepsilon}_f(t) - C_1^2\frac{\mathrm{d}\varepsilon_p(\Phi(t))}{\mathrm{d}\Phi(t)} \tag{16}$$

in another form. Associating Eqs. (11), (14) and (16), we obtain a differential equation

$$\frac{\dot{\varepsilon}_f(t)}{\varepsilon_f(t)} = -\frac{E_1/C_1}{m + \rho_0 C_1(t-t_1)}. \tag{17}$$

Integrating the above relation, we have the strain behind the front

$$\varepsilon_f(t) = \frac{m\varepsilon_f(t_1+0)}{m + \rho_0 C_1(t-t_1)}, \tag{18}$$

in which $\varepsilon_f(t_1+0)$ is still unknown but it can be determined as follows. Substituting Eq. (18) in Eq. (15) with $t = t_1+0$ and $\Phi(t_1+0) = 0$, we have

$$v_b(t_1+0) = C_1\varepsilon_f(t_1+0) - V_0 + C_1\frac{\sigma_0}{E_1}\ln(1+\mu). \tag{19}$$

Since $v_b(t_1+0) = v_b(t_1)$ which is shown in Eq. (9), we can derive

$$\varepsilon_f(t_1+0) = 2\left[\frac{V_0}{C_1} - \frac{\sigma_0}{E_1}\ln(1+\mu)\right] = 2\varepsilon_p(0).$$

This means that the reflected wave leads to the strain at the distal end being doubled. At the time before the reflected wave reaches the proximal end, i.e. $t < t_2 = 2l_0/C_1$, the strain and stress behind the front are expressed as

$$\varepsilon_f(t) = \frac{2m}{m + \rho_0 C_1(t-t_1)}\left[\frac{V_0}{C_1} - \frac{\sigma_0}{E_1}\ln(1+\mu)\right] \tag{20}$$

and

$$\sigma_f(t) = \sigma_0 + \frac{2m(\rho_0 V_0 C_1 - \sigma_0\ln(1+\mu))}{m + \rho_0 C_1(t-t_1)}, \tag{21}$$

respectively. So, the physical quantities in the rod at position X and time t are expressed as

$$\{\bar{v},\bar{\varepsilon},\bar{\sigma}\} = \begin{cases} \left\{v_b(t),\varepsilon_f(t_1+X/C_1),\sigma_f(t)\right\}, & 0 \le X < C_1(t-t_1) \\ \{0,\varepsilon_p(X),\sigma_p(C_1(t-t_1))\}, & C_1(t-t_1) < X \le l_0 \end{cases}. \tag{22}$$

The components in Eq. (22) can be easily determined from Eqs. (10), (11), (15), (20) and (21).

However, if the rod deforms in the *Shock Mode* after wave reflection, we have $\varepsilon_f(t) = \varepsilon_L$ according to the R-LHP-L idealisation. Using $a_b(t) = \dot{v}_b(t)$ with Eq. (15), we obtain

$$-\frac{\sigma_f(t)}{m + \rho_0\Phi(t)} = \ddot{\Phi}(t)\left(\varepsilon_L - \varepsilon_p(\Phi(t))\right) - \left(\dot{\Phi}(t)\right)^2\frac{\mathrm{d}\varepsilon_p(\Phi(t))}{\mathrm{d}\Phi(t)}. \tag{23}$$

From the kinematic and kinetic compatibility conditions across the shock front, we have

$$\sigma_f(t) - \sigma_p(\Phi(t)) = \rho_0\left(\dot{\Phi}(t)\right)^2\left(\varepsilon_L - \varepsilon_p(\Phi(t))\right), \tag{24}$$

which leads to a differential equation for the position of the shock front

$$\ddot{\Phi}(t) = \frac{1}{m+\rho_0\Phi(t)}\left[\frac{\left(\dot{\Phi}(t)/C_1\right)^2\sigma_0 - (\sigma_0 + E_1\varepsilon_L)}{\varepsilon_L - \frac{V_0}{C_1} - \frac{\sigma_0}{E_1}\ln\frac{m+\rho_0\Phi(t)}{m+\rho_0 l_0}} + \rho_0 C_1^2 - \rho_0\left(\dot{\Phi}(t)\right)^2\right] \tag{25}$$

with $\Phi(t_1) = 0$ and $\dot{\Phi}(t_1+0) = v_b(t_1)/(\varepsilon_L - v_b(t_1)/C_1)$. A method of numerical integration such as the fourth-order Runge–Kutta numerical scheme can be used to solve this differential equation. Thus, the physical quantities in the rod at position X and time t

$$\{\bar{v},\bar{\varepsilon},\bar{\sigma}\} = \begin{cases} \left\{v_b(t),\varepsilon_L,\sigma_f(t)\right\}, & 0 \le X < \Phi(t) \\ \{0,\varepsilon_p(X),\sigma_p(\Phi(t))\}, & \Phi(t) < X \le l_0 \end{cases} \tag{26}$$

can be calculated.

3.1.2. High velocity impact

For a high velocity impact, the rod deforms in the *Shock Mode* during the propagation of plastic shock front from the proximal end to the distal end. According to the R-LHP-L idealisation, the strain behind the shock front is $\varepsilon_f(t) = \varepsilon_L$. From the kinematic compatibility condition across the shock front Eq. (3), we have $v_b(t) = -\dot{\Phi}(t)\varepsilon_L$, which leads to $a_b(t) = -\ddot{\Phi}(t)\varepsilon_L$. Associating this result with Eq. (1), we obtain a differential equation

$$\ddot{\Phi}(t) = \frac{\sigma_0/\varepsilon_L}{m + \rho_0\Phi(t)}. \tag{27}$$

To solve this equation, multiply both sides by $\dot{\Phi}(t)$ and integrate with the initial condition $\dot{\Phi}(0) = -V_0/\varepsilon_L$ and $\Phi(0) = l_0$. In this process, we first obtain the wave speed

$$\dot{\Phi}(t) = -\frac{V_0}{\varepsilon_L}\left[1 + \frac{2\sigma_0\varepsilon_L}{\rho_0 V_0^2}\ln\frac{m+\rho_0\Phi(t)}{m+\rho_0 l_0}\right]^{1/2}, \tag{28}$$

and then have the time

$$t = \frac{\varepsilon_L}{V_0}\int_{\Phi(t)}^{l_0}\left[1+\frac{2\sigma_0\varepsilon_L}{\rho_0 V_0^2}\ln\frac{m+\rho_0 X}{m+\rho_0 l_0}\right]^{-1/2}\mathrm{d}X. \tag{29}$$

The above equation can be rewritten as

$$t = \frac{m\varepsilon_L(1+\mu)\sqrt{2\pi\alpha}}{2\rho_0 V_0\exp(\alpha/2)}\left[erfi\left(\sqrt{\alpha/2}\right)-erfi(\eta)\right] \tag{30}$$

with

$$\alpha = \left(\rho_0 V_0^2/\varepsilon_L\right)\Big/\sigma_0 \tag{31}$$

and

$$\eta = \left(\frac{\alpha}{2}+\ln\frac{m+\rho_0\Phi(t)}{m+\rho_0 l_0}\right)^{1/2}, \tag{32}$$

where α is a dimensionless parameter, namely the shock-enhancement parameter, and $erfi(x) = 2\pi^{-1/2}\int_0^x e^{s^2}\mathrm{d}s$ the imaginary error function. So, we can have

$$\Phi(t) = \frac{m}{\rho_0}\left\{(1+\mu)\exp\left[\left(erfi^{-1}(\tau)\right)^2-\frac{\alpha}{2}\right]-1\right\} \tag{33}$$

and

$$\dot{\Phi}(t) = -\sqrt{2\sigma_0/\rho_0\varepsilon_L}\,erfi^{-1}(\tau), \tag{34}$$

in which

$$\tau = erfi\left(\sqrt{\alpha/2}\right) - \frac{\exp(\alpha/2)}{\sqrt{2\pi\alpha}(1+\mu)}\frac{2\rho_0 V_0 t}{m\varepsilon_L}, \tag{35}$$

where $erfi^{-1}(\tau)$ is the inverse of the imaginary error function, which is determined by solving $erfi(\eta) = \tau$ through Newton's method. The stress behind the shock front is

$$\sigma_f(t) = \sigma_0+\rho_0\left(\dot{\Phi}(t)\right)^2\varepsilon_L = \sigma_0+2\sigma_0\left(erfi^{-1}(\tau)\right)^2. \tag{36}$$

By taking $t = 0$, Eq. (35) leads to $\tau = erfi(\sqrt{\alpha/2})$. From this and Eqs. (31) and (36), it can be proved that the *initial* stress behind the shock front is

$$\sigma_f(0) = \sigma_0+\rho_0 V_0^2/\varepsilon_L, \tag{37}$$

which varies proportionally with the *square* of the impact velocity when the cellular material is deformed in the *Shock Mode*. This prediction is consistent with the results of Harrigan et al. [10], Ruan et al. [4], Tan et al. [3]and Li et al. [24]. The physical quantities in the rod at position X and time t are expressed as

$$\{\bar{v},\bar{\varepsilon},\bar{\sigma}\} = \begin{cases}\left\{-\dot{\Phi}(t)\varepsilon_L, 0, \sigma_0\right\}, & 0\le X<\Phi(t)\\ \left\{0,\varepsilon_L,\sigma_f(t)\right\}, & \Phi(t)<X\le l_0\end{cases} \tag{38}$$

with $\dot{\Phi}(t)$ and $\sigma_f(t)$ in Eqs. (34) and (36), respectively. We denote this model as the Shock-Mode model.

If the stress behind the shock front reduces to $\sigma_0+E_1\varepsilon_L$ before the wave reaches the distal end, a mode transition from the *Shock Mode* to the *Transitional Mode* will occur. The corresponding transformation time and position of the shock front can be determined as

$$t_{S-T} = \frac{m\varepsilon_L(1+\mu)\sqrt{2\pi\alpha}}{2\rho_0 V_0\exp(\alpha/2)}\left[erfi\left(\sqrt{\alpha/2}\right)-erfi\left(\sqrt{\beta/2}\right)\right] \tag{39}$$

and

$$\Phi_{S-T} = \Phi(t_{S-T}) = \frac{m}{\rho_0}[(1+\mu)\exp(\beta/2-\alpha/2)-1], \tag{40}$$

respectively, where

$$\beta = E_1\varepsilon_L/\sigma_0 \tag{41}$$

is a dimensionless parameter, namely the *stress-hardening* parameter. After the mode transition, the position of the shock front is

$$\Phi(t) = \Phi_{S-T}-C_1(t-t_{S-T}). \tag{42}$$

The acceleration and velocity of the mass are

$$a_b(t) = -\frac{\sigma_0}{m+\rho_0(\Phi_{S-T}-C_1(t-t_{S-T}))} \tag{43}$$

and

$$v_b(t) = C_1\varepsilon_L+C_1\frac{\sigma_0}{E_1}\ln\frac{m+\rho_0(\Phi_{S-T}-C_1(t-t_{S-T}))}{m+\rho_0\Phi_{S-T}}, \tag{44}$$

respectively. The physical quantities behind the shock front are expressed as

$$\varepsilon_f(t) = -v_b(t)/\dot{\Phi}(t) = v_b(t)/C_1, \tag{45}$$

$$v_f(t) = -v_b(t) = \dot{\Phi}(t)\varepsilon_f(t) = -C_1\varepsilon_f(t), \tag{46}$$

$$\sigma_f(t) = \sigma_0+E_1\varepsilon_f(t). \tag{47}$$

The physical quantities in the rod at position X and time t are expressed as

$$\{\bar{v},\bar{\varepsilon},\bar{\sigma}\} = \begin{cases}\{v_b(t),0,\sigma_0\}, & 0\le X<\Phi(t)\\ \left\{0,\varepsilon_f(t_{S-T}+(\Phi_{S-T}-X)/C_1),\sigma_f(t)\right\}, & \Phi(t)<X\le\Phi_{S-T}\\ \left\{0,\varepsilon_L,\sigma_f(t)\right\}, & \Phi_{S-T}\le X\le l_0\end{cases} \tag{48}$$

in which

$$\varepsilon_f(t_{S-T}+(\Phi_{S-T}-X)/C_1) = \varepsilon_L+\frac{\sigma_0}{E_1}\ln\frac{m+\rho_0 X}{m+\rho_0\Phi_{S-T}}. \tag{49}$$

3.2. The striker-rod impact scenario

3.2.1. Moderate velocity impact

When the rod is impacted by a rigid mass with a moderate velocity, it deforms in the *Transitional Mode*. Similarly, we can present the Transitional-Mode model with the physical quantities in the rod at position X and time t as

$$\{\bar{v},\bar{\varepsilon},\bar{\sigma}\} = \begin{cases}\{v_b(t),v_b(X/C_1)/C_1,\sigma_0+E_1 v_b(t)/C_1\}, & 0\le X<C_1 t\\ \{0,0,\sigma_0\}, & C_1 t<X\le l_0\end{cases} \tag{50}$$

in which

$$v_b(t) = C_1\frac{mV_0-\sigma_0 t}{mC_1+E_1 t}. \tag{51}$$

At time $t_1 = l_0/C_1$, the wave front reaches the distal end.

When the wave is reflected back from the distal end, if the rod is deformed in the *Transitional Mode*, we can determine the velocity of the mass as

$$v_b(t) = \frac{(1-\mu)\sigma_0 + 2\rho_0 V_0 C_1}{(1+\mu)\rho_0 C_1} - \frac{V_0 + C_1\sigma_0/E_1}{1+\mu(2-C_1 t/l_0)}, \tag{52}$$

and the physical quantities in the rod at position X and time t as

$$\{\overline{v},\overline{\varepsilon},\overline{\sigma}\} = \begin{cases} \left\{v_b(t), \dfrac{mV_0C_1-\sigma_0 X}{(m+\rho_0 X)C_1^2}, \dfrac{\sigma_0+E_1V_0/C_1}{1+\mu(2-C_1t/l_0)}\right\}, & 0 \le X < \Phi(t) \\ \left\{0, \dfrac{2}{1+\mu}\left(\dfrac{V_0}{C_1} - \dfrac{\sigma_0 l_0}{mC_1^2}\right), \dfrac{(1-\mu)\sigma_0+2\rho_0V_0C_1}{1+\mu}\right\}, & \Phi(t) < X \le l_0 \end{cases} \tag{53}$$

in which $\Phi(t) = 2l_0 - C_1 t$. It is interesting that the strain and stress behind the wave front are constant. But if the rod is deformed in the *Shock Mode*, we can determine the shock velocity as

$$\dot{\Phi}(t) = -C_1\left\{1 + \frac{\left[2\sqrt{\alpha\beta} - 2\mu - (1+\mu)\beta\right]\beta(1+\mu\Phi(t)/l_0)^2}{(1+\mu)\left[\left(\beta - \sqrt{\alpha\beta}\right) + (1+\beta)\mu\Phi(t)/l_0\right]^2}\right\}^{1/2}. \tag{54}$$

and so we can calculate the time when the shock front reaches the position $\Phi(t)$

$$t = t_1 + \int_{\Phi(t)}^{l_0} \frac{1}{\dot{\Phi}(t)} d\Phi(t). \tag{55}$$

The physical quantities in the rod at position X and time t can be determined as

$$\{\overline{v},\overline{\varepsilon},\overline{\sigma}\} = \begin{cases} \left\{-\dot{\Phi}(t)\left(\varepsilon_L - \varepsilon_p(\Phi(t))\right), \varepsilon_p(X), \sigma_p(\Phi(t))\right\}, & 0 \le X < \Phi(t) \\ \left\{0, \varepsilon_L, \sigma_p(\Phi(t)) + \rho_0\left(\dot{\Phi}(t)\right)^2\left(\varepsilon_L - \varepsilon_p(\Phi(t))\right)\right\}, & \Phi(t) < X \le l_0 \end{cases} \tag{56}$$

in which

$$\sigma_p(X) = \frac{m(E_1V_0 + \sigma_0 C_1)}{C_1(m+\rho_0 X)}, \tag{57}$$

$$\varepsilon_p(X) = \frac{mV_0C_1 - \sigma_0 X}{C_1^2(m+\rho_0 X)}. \tag{58}$$

3.2.2. High velocity impact

When the rod is impacted by a rigid mass with a high velocity, it deforms in the *Shock Mode*. Similarly, we can present the Shock-Mode model with the physical quantities in the rod at position X and time t as

$$\{\overline{v},\overline{\varepsilon},\overline{\sigma}\} = \begin{cases} \left\{v_b(t), \varepsilon_L, \sigma_0 + \rho_0(v_b(t))^2/\varepsilon_L\right\}, & 0 \le X < \Phi(t) \\ \{0, 0, \sigma_0\}, & \Phi(t) < X \le l_0 \end{cases} \tag{59}$$

in which

$$v_b(t) = \frac{V_0 - \sigma_0 t/m}{\left[1 + (2mV_0 - \sigma_0 t)\rho_0 t/m^2\varepsilon_L\right]^{1/2}}, \tag{60}$$

$$\Phi(t) = \frac{m}{\rho_0}\left\{-1 + \left[1 + (2mV_0 - \sigma_0 t)\rho_0 t/m^2\varepsilon_L\right]^{1/2}\right\}. \tag{61}$$

If there is a mode transition in the crushing process, the transformation time t_{S-T} can be determined as

$$t_{S-T} = \frac{mV_0}{\sigma_0}\left[1 - \sqrt{\frac{1+\alpha^{-1}}{1+\beta^{-1}}}\right], \tag{62}$$

and the corresponding position of the shock front can be determined as

$$\Phi_{S-T} = \frac{m}{\rho_0}\left[-1 + \sqrt{\frac{1+\alpha}{1+\beta}}\right], \tag{63}$$

where α and β are two dimensionless parameters defined by Eqs. (31) and (41), respectively. After the mode transition, the wave speed is reduced to $\dot{\Phi}(t) = C_1$, so the front position is written as

$$\begin{aligned} \Phi(t) &= \Phi_{S-T} + C_1(t - t_{S-T}) \\ &= \frac{m}{\rho_0}\left[\sqrt{(1+\alpha)(1+\beta)} - \sqrt{\alpha\beta} - 1\right] + C_1 t. \end{aligned} \tag{64}$$

The physical quantities in the rod at position X and time t are expressed as

$$\{\overline{v},\overline{\varepsilon},\overline{\sigma}\} = \begin{cases} \{v_b(t), \varepsilon_L, \sigma_0 + E_1 v_b(t)/C_1\}, & 0 \le X \le \Phi_{S-T} \\ \{v_b(t), v_b(\tau)/C_1, \sigma_0 + E_1 v_b(t)/C_1\}, & \Phi_{S-T} < X < \Phi(t) \\ \{0, 0, \sigma_0\}, & \Phi(t) < X \le l_0 \end{cases} \tag{65}$$

where $\tau = t_{S-T} + (X - \Phi_{S-T})/C_1$ and

$$v_b(t) = \frac{C_1(mV_0 - \sigma_0 t)}{mC_1\sqrt{(1+\alpha)(1+\beta)} - mV_0E_1/\sigma_0 + E_1 t}. \tag{66}$$

The above equation can be easily determined from Eq. (51) by taking V_0, m and t as $C_1\varepsilon_L$, $m+\rho_0\Phi_{S-T}$ and $t-t_{S-T}$, respectively.

4. Comparison and discussion

4.1. The relationship between the Shock-Mode model and the R-P-P-L model

The Shock-Mode model in this study is essentially the same as the R-P-P-L model presented by Tan et al. [3]. However, there are still some subtle differences between these two models. First, the R-P-P-L model used a thermo-mechanical approach to form the governing equations but the Shock-Mode model is derived from the stress wave theory. Second, the definitions of the material parameters such as the yield stress are different because of the different idealisations. Third, the present theoretical predictions are much simpler, as discussed below.

For the rod-target impact scenario, the Shock-Mode model is constructed in Section 3.1.2 and from Eq. (38) we have the velocity and the stress behind the shock front

$$\overline{v} = \sqrt{2\sigma_0\varepsilon_L/\rho_0}\, erfi^{-1}(\tau) \tag{67}$$

and

$$\overline{\sigma} = \sigma_0 + 2\sigma_0\left(erfi^{-1}(\tau)\right)^2, \tag{68}$$

respectively, in which τ varies linearly with the time t, see Eq. (35). Hence, these two results can be easily calculated when the algorithms of the imaginary error function and its inverse are available. However, Tan et al. [3]gave the velocity and the stress behind the shock front as

$$\bar{v} = \dot{u}_{l_0} = \left\{V_0^2 + 2\sigma^{qs}\varepsilon_D \ln\left(1 - u_{l_0}/(1+M_r)\varepsilon_D l_0\right)/\rho_0\right\}^{1/2}, \tag{69}$$

and

$$\bar{\sigma} = \sigma^d = \sigma^{qs}\left\{1 + 2\ln\left(1 - u_{l_0}/(1+M_r)\varepsilon_D l_0\right)\right\} + \rho_0 V_0^2/\varepsilon_D. \tag{70}$$

respectively, where σ^{qs} is the quasi-static 'plateau' stress (In Ref. [3], σ^{qs} was defined as the quasi-static yield stress, but this difference could not be distinguished in the R-P-P-L idealisation.) and $M_r = M_b/\rho_0 A_0 l_0$ the mass ratio. In Ref. [3], the displacement of the distal end of the foam rod u_{l0} needs to be determined by using a numerical method (e.g. a fourth-order Runge–Kutta numerical scheme) to solve Eq. (69). In fact, using $u_{l0} = \varepsilon_D(l_0 - \Phi(t))$ and $\varepsilon_L = \varepsilon_D$ with $\Phi(t)$ in Eq. (33), we can simplify Eqs. (69) and (70) to Eqs. (67) and (68), respectively.

For the striker-rod impact scenario, the Shock-Mode model is constructed in Section 3.2.2 and from Eq. (59) we have the velocity and the stress behind the shock front

$$\bar{v} = V_0 \frac{1 - \sigma_0 t/mV_0}{\left[1 + (2mV_0 - \sigma_0 t)\rho_0 t/m^2\varepsilon_L\right]^{1/2}} \tag{71}$$

and

$$\bar{\sigma} = \sigma_0 + \frac{\rho_0 V_0^2}{\varepsilon_L}\frac{(1 - \sigma_0 t/mV_0)^2}{1 + (2mV_0 - \sigma_0 t)\rho_0 t/m^2\varepsilon_L}, \tag{72}$$

respectively. These two predictions are explicit. However, Tan et al. [3]presented the velocity and the stress behind the shock front by

$$\bar{v} = \dot{u}_{l_0} = \left\{\varepsilon_D\left(M_r^2\left(\sigma^{qs} + \rho_0 V_0^2/\varepsilon_D\right)\Big/\left(M_r + u_{l_0}/\varepsilon_D l_0\right)^2 - \sigma^{qs}\right)\Big/\rho_0\right\}^{1/2} \tag{73}$$

and

$$\bar{\sigma} = \sigma^d = M_r^2\left(\sigma^{qs} + \rho_0 V_0^2/\varepsilon_D\right)\Big/\left(M_r + u_{l_0}/\varepsilon_D l_0\right)^2, \tag{74}$$

respectively. In their study, the displacement of the proximal end of the foam rod u_{l0} needs to be determined by using a numerical method to solve Eq. (73). In fact, using $u_{l0} = \varepsilon_D\Phi(t)$ and $\varepsilon_L = \varepsilon_D$ with $\Phi(t)$ in Eq. (61), we can simplify Eqs. (73) and (74) to Eqs. (71) and (72), respectively.

4.2. Features of the theoretical predictions

According to the R-LHP-L idealisation, when $\sigma_f(0)$ presented in Eq. (37) is greater than $\sigma(\varepsilon_L)$, the *Shock Mode* occurs, so we have

$$\sigma_0 + \rho_0 V_0^2/\varepsilon_L \geq \sigma_0 + E_1\varepsilon_L. \tag{75}$$

When the equality sign is attained in the above equation, this gives the *second* critical velocity, i.e. the critical impact velocity for mode transition from *Shock Mode* to the *Transitional Mode*

$$V_{c2} = \varepsilon_L\sqrt{E_1/\rho_0} = C_1\varepsilon_L. \tag{76}$$

To determine the *first* critical impact velocity, i.e. the critical impact velocity for mode transition from the Homogenous Mode to the *Transitional Mode*, we employ the Stress Uniformity Index [6,25]

$$\mathrm{SUI} = \sigma_{pl}^s/\sigma_{pl}^i, \tag{77}$$

which characterise the degree of uniformity between the plateau stress on the impact surface σ_{pl}^i and the plateau stress on the support surface σ_{pl}^s. The stress in the foam rod is almost uniform when the value of SUI is up to 90%, say. Hence, we take SUI = 90% to determine the first critical impact velocity. Since $\sigma_{pl}^i = \sigma_f(0)$ and $\sigma_{pl}^s = \sigma_0$ with $\sigma_f(0)$ in Eq. (7) and $V_0 = V_{c1}$, we have the first critical impact velocity

$$V_{c1} = \sigma_0/9\rho_0 C_1. \tag{78}$$

In fact, these two critical impact velocities are valid for both impact scenarios to predict the initial deformation mode. The mode transition from the *Transitional Mode* to the Homogeneous Mode may appear during the crushing process, but we do not discuss this transition below because the model for deformation in the Homogeneous Mode is not available in the present theoretical framework.

We have defined two new and useful dimensionless parameters. One is the shock-enhancement parameter α, which characterizes the ratio of the shock-enhancement induced by inertia, $\rho_0 V_0^2/\varepsilon_L$, to the yield stress, σ_0, as defined in Eq. (31). The other is the stress-hardening parameter β, which characterizes the ratio of the hardening part of stress at locking, $E_1\varepsilon_L$, to the yield stress, σ_0, as defined in Eq. (41).

To describe some features of the theoretical predictions, consider the striker-rod impact scenario for an infinite rod length. The theoretical predictions of this impact scenario show that the impact response in the *Shock Mode* is independent of the stress-hardening parameter β and after the mode transition the impact response in the *Transitional Mode* depends on both parameters, α and β. The corresponding features are discussed below.

Firstly, the influences of the stress-hardening parameter β on the physical quantities at the proximal end and at the shock front are investigated. The shock-enhancement parameter α is fixed as 5 and the stress-hardening parameter β is taken as a series of values (0.1, 0.2, 0.5, 1, 2, 5 and 10). For all these cases, the corresponding physical quantities, except the strain behind the shock front in the *Shock Mode*, decrease with increasing time, as shown in Fig. 4. The stress behind the shock front in the *Shock Mode* decreases faster than that in the *Transitional Mode*, but the velocity at the shock front in the *Shock Mode* decreases more slowly than that in the *Transitional Mode*. For $\beta > 5$, the rod is crushed in the *Transitional Mode*. For $\beta < 5$, the rod is crushed first in the *Shock Mode* and then in the *Transitional Mode*, and the dimensionless transformation time increases with the decrease of the stress-hardening parameter β.

Secondly, the influence of the shock-enhancement parameter α on the physical quantities behind the shock front is investigated. The stress-hardening parameter β is fixed as 1 and the shock-enhancement parameter α is taken as a series of values (0.1, 0.2, 0.5, 1, 2, 5, 10, 20 and 50). For all these cases, the corresponding physical quantities, except the strain behind the shock front in the *Shock Mode*, decrease with increasing time, as shown in Fig. 5. In Fig. 6(a) and (c), the regions are divided into two parts by the line of mode transition. For $\alpha < 1$, the rod is crushed in the *Transitional Mode*. For $\alpha > 1$, the rod is crushed first in the *Shock Mode* and then in the *Transitional Mode*, and the dimensionless transformation time increases with the increase of the shock-enhancement parameter α.

Finally, the stress and strain distributions for the case of $\alpha = 5$ and $\beta = 1$ are plotted in three-dimensional diagrams and two-dimensional diagrams, see Fig. 6. In the figure, the dimensionless time is defined as $t^* = \sigma_0 t/mV_0$. For this case, the rod is crushed first in the *Shock Mode* and then in the *Transitional Mode*. The dimensionless transformation time, t_{S-T}^*, is about 0.225. It is shown that the stress increases along the rod behind the shock but the strength of the plastic loading wave decreases with increasing time. At the shock front, there exists a jump, ahead of which there is an elastic loading wave spreading to the distal end of the foam rod. In the current idealisation, the speed of elastic wave is infinite. The strain changes markedly in the crushing process.

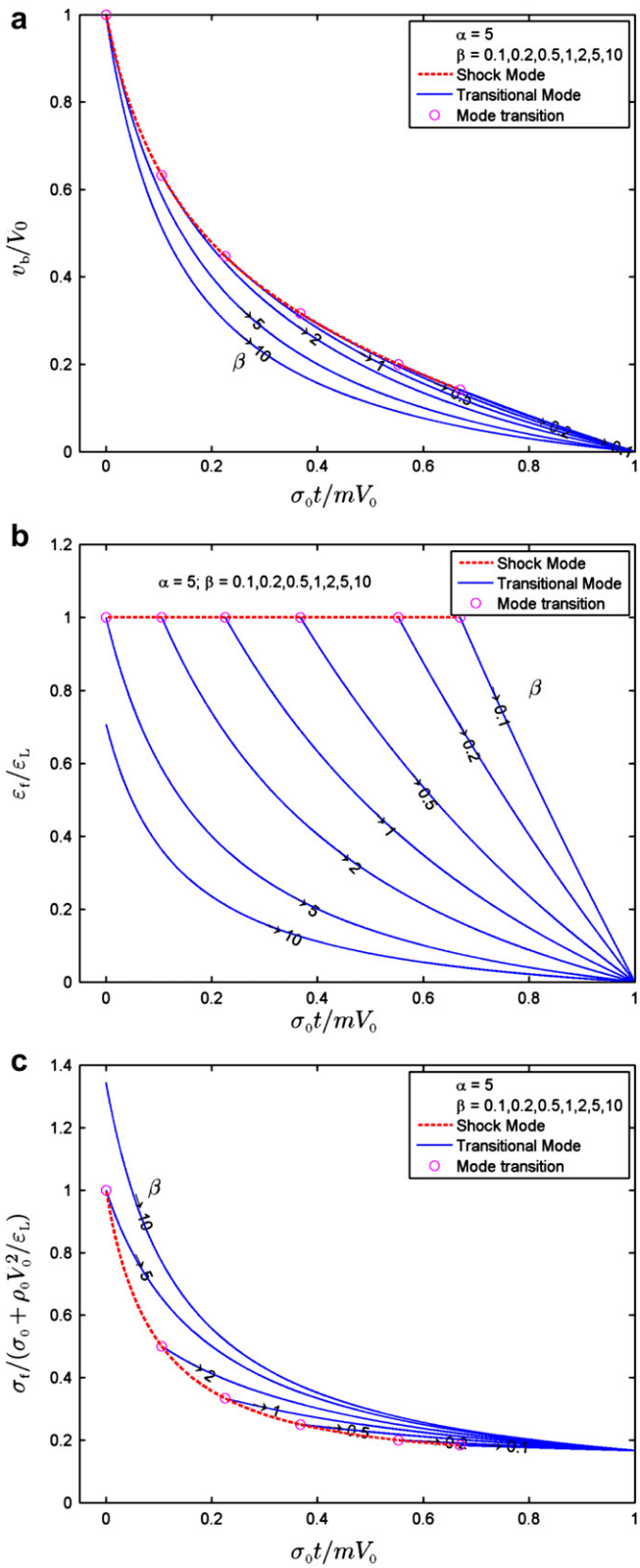

Fig. 4. The features of the physical quantities behind the shock front with $\alpha = 5$ and $\beta = 0.1, 0.2, 0.5, 1, 2, 5$ and 10.

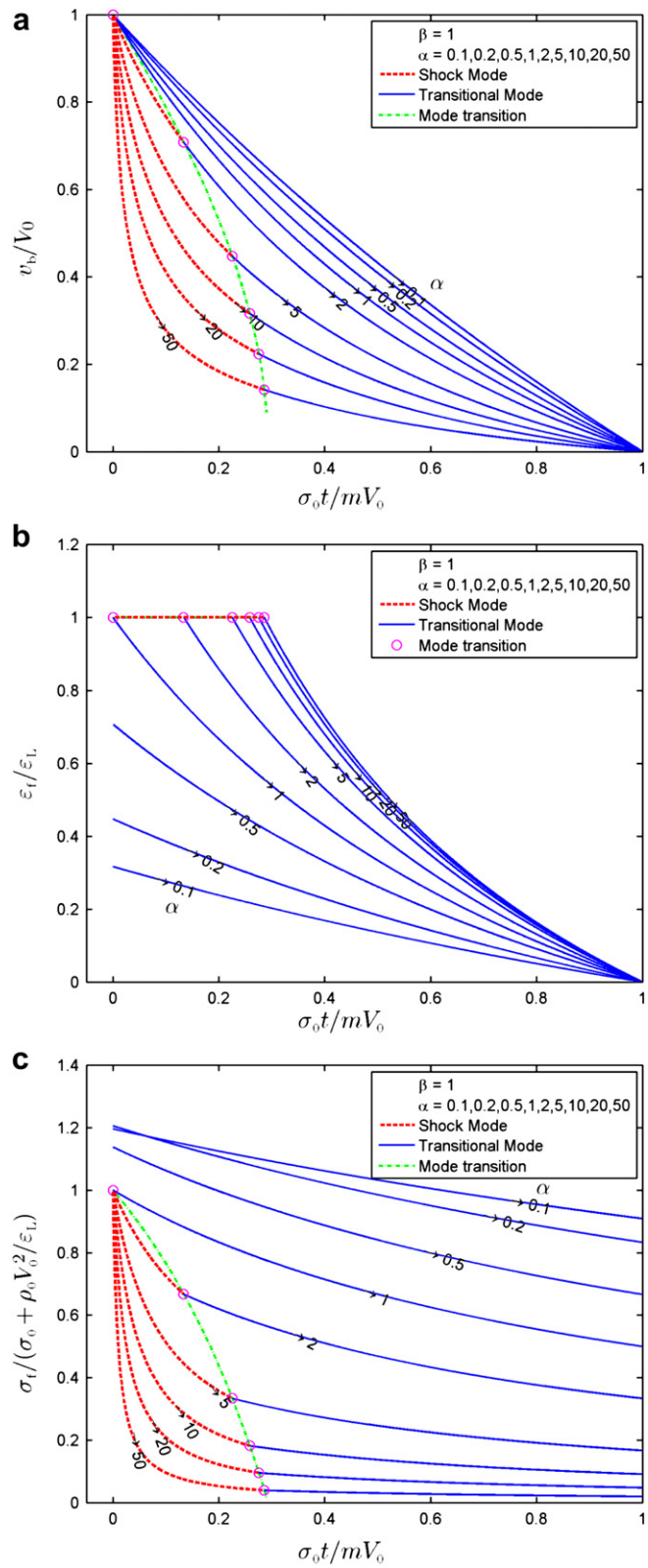

Fig. 5. The features of the physical quantities ahead of the shock front with $\beta = 1$ and $\alpha = 0.1, 0.2, 0.5, 1, 2, 5, 10, 20$ and 50.

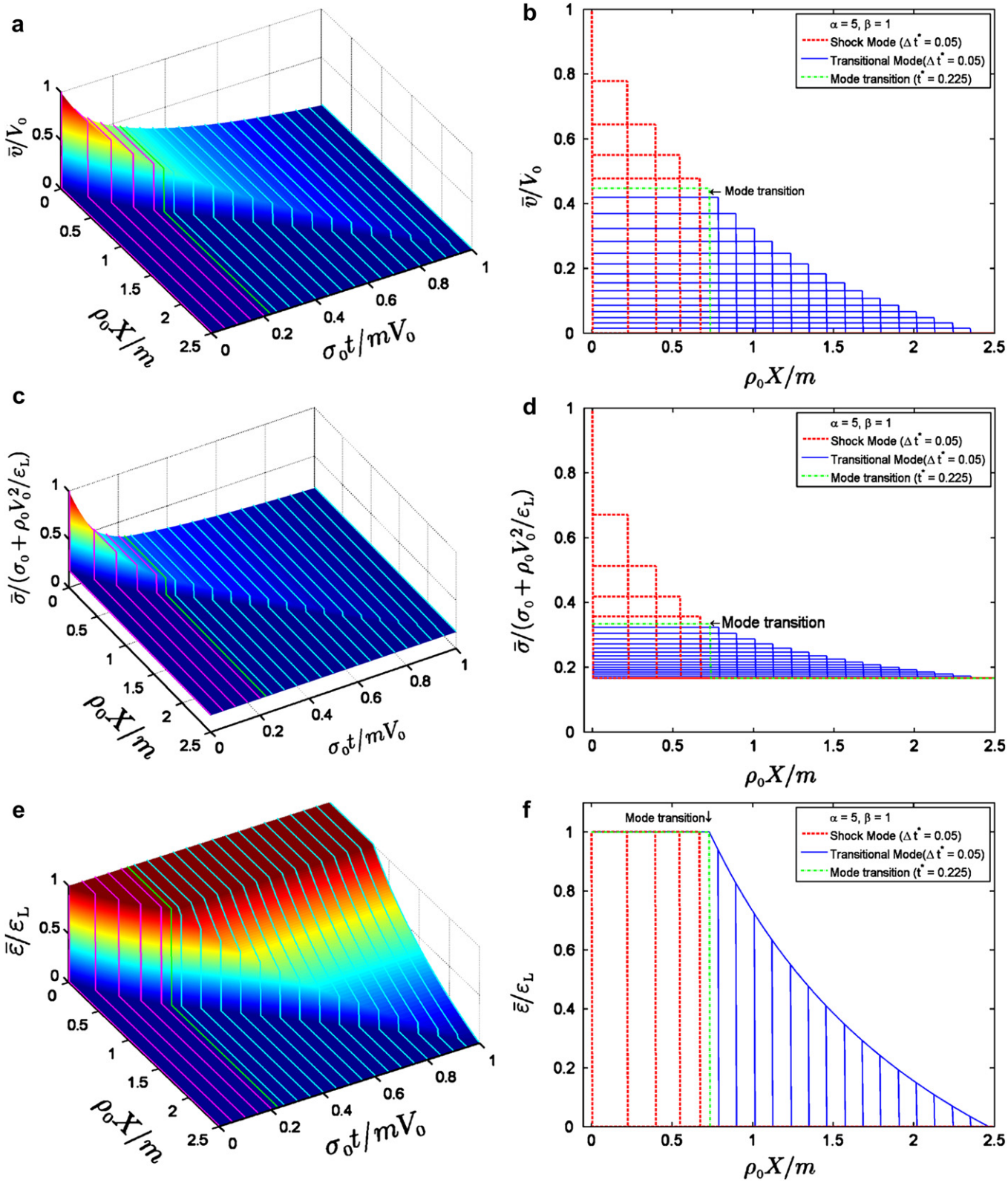

Fig. 6. The distributions of velocity, stress and strain of a case of $\alpha = 5$ and $\beta = 1$. (a) Velocity-X-t, (b) Velocity-X, (c) Stress-X-t, (d) Stress-X, (e) Strain-X-t, and (f) Strain-X.

4.3. Comparison with the experimental results of Hydro/Cymat foams in Ref. [2]

In this section, the validity of the theoretical predictions will be verified by compared with the experimental results taken from the literature [2]. Quasi-static and dynamic compression tests of closed cell Hydro/Cymat foams were carried out by Tan et al. [2]. The foams with the relative density of ~0.1 have closed cells with a mean cell diameter of ~4 mm and their solid ligaments are made of the Al–Si(7–9%)–Mg(0.5–1%) alloy with the density ρ_s of

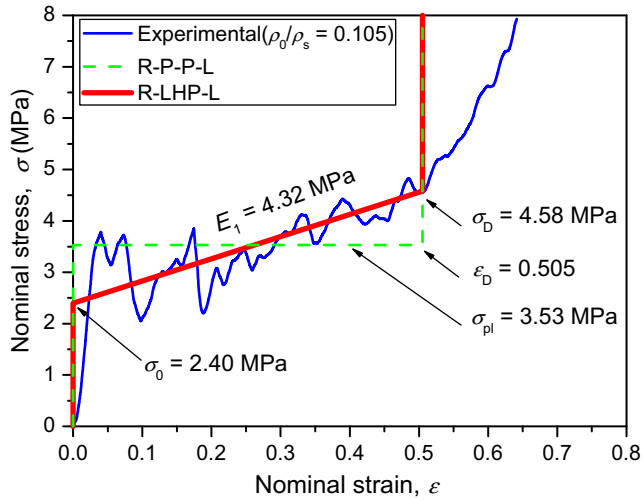

Fig. 7. The quasi-static stress-strain curve and the corresponding R-P-P-L and R-LHP-L idealisations. The experimental data was taken from Ref. [2].

2730 kg/m^3. The specimens were 45 mm in diameter and 45 mm in length. The dynamic crushing of the rod-target impact scenario was carried out on an experimental set-up for direct impact testing of aluminium foam projectiles. The material parameters for the theoretical modelling are needed from the quasi-static compression results. A quasi-static stress-strain curve taken from Fig. 8a in Ref. [2] is shown in Fig. 7. The relative density of this foam specimen is 0.105 and the loading direction is along the *y* direction, transverse to the casting direction, see Fig. 1 in Ref. [2].

Theoretically, according to the 1D stress wave theory, for a material with a stress-strain curve like foam materials (for example, the experimental curve shown in Fig. 7), a shock wave will propagate in a bar at high velocity impact. The strain behind the wave front depends on the stress jump. In the case of a mass impact, as the shock wave propagates, the magnitude of the stress decreases and so the strain behind the wave front will also get smaller. In the case of a constant velocity impact, the strain behind the wave front is constant and related to the impact velocity. So, the strain behind the wave front is velocity-sensitive. This could be of interest to researchers. For simplicity, a constant strain, i.e. the locking strain [1,3], is assumed to approximate the strain behind the wave front because its value varies within a small range. In our model, the locking strain will be taken as the densification strain ε_D as assumed by Tan et al. [3]. This is an approximation and the question on the choice of its value remains open as noted above. The R-P-P-L and R-LHP-L idealisations of the experimental curve are also shown in Fig. 7. The R-P-P-L idealisation has $\sigma_{pl} = 3.53$ MPa and $\varepsilon_D = 0.505$ as its parameters. The R-LHP-L idealisation has $\sigma_0 = 2.40$ MPa, $E_1 = 4.32$ MPa and $\varepsilon_D = 0.505$ as its parameters. We use these parameters for the models in the following discussion, i.e. we neglect the slight difference of the relative density ($\sim$0.1) of the foam specimens used.

A comparison of the load at the proximal end of the foam rod between theoretical predictions and experimental results [2] is shown in Fig. 8. Three different cases of the initial impact velocities $V_0 = 13.4$, 50.0 and 109.2 m/s with corresponding masses $M_b = 0.403$, 0.117 and 0.051 kg are considered. For the crushing in the *Transitional Mode*, good agreement is achieved. For the crushing in the *Shock Mode*, most features of the load-time curve described above are correctly predicted but the accuracy of the theoretical predictions is not high. This is probably due to the simplicity of the definition of the locking stage of the constitutive behaviour. Although different idealisations were employed to develop the present models and the R-P-P-L model, some predictions such as the load at the proximal end and the velocity of the mass (see Fig. 9a) are almost at the same levels. However, the deformation in the foam rod predicted by the present models is very different from that of the classic R-P-P-L model when the impact velocity is not high, as discussed below.

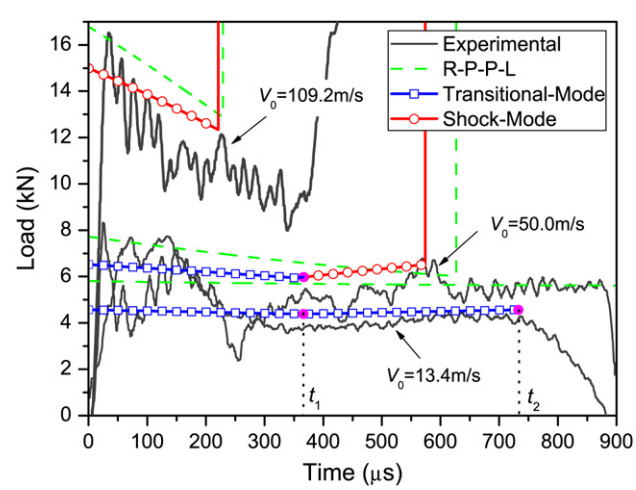

Fig. 8. Comparison of the load at the proximal end of the foam rod between theoretical predictions and experimental results. The experimental data was taken from Ref. [2].

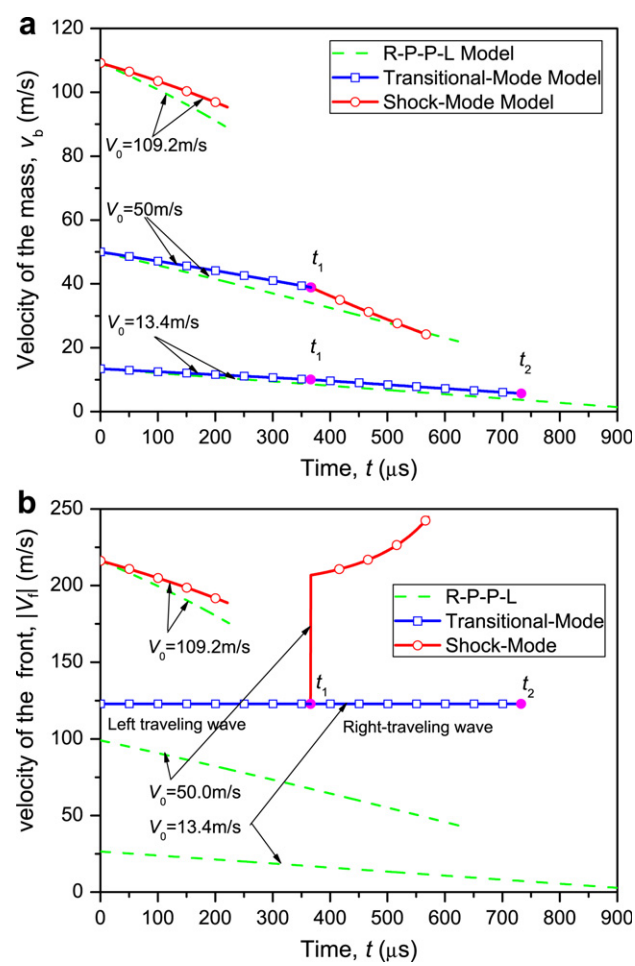

Fig. 9. Variations of (a) the velocity of the mass and (b) the Lagrangian velocity of the front.

A comparison of the Lagrangian velocity of the front is shown in Fig. 9b. From the R-P-P-L predictions for all the cases of initial impact velocities, a shock front with diminishing velocity travels from the proximal end to the distal end. Similar behaviour is found in the prediction by the Shock-Mode model for the case of $V_0 = 109.2$ m/s. But for the cases of $V_0 = 13.4$ m/s and 50.0 m/s, the predictions by the present models show that the front is reflected back from the distal end.

Strain distributions in the foam rod at time 0.1 ms and 0.4 ms are also calculated, as shown in Fig. 10. We first discuss the theoretical predictions by using the R-LHP-L idealisation, see Fig. 10b. For the cases of $V_0 = 13.4$ and 50.0 m/s, a front propagates from the proximal end to the distal end and then is reflected back from the distal end. As the front propagates, the strain behind the front reduces for both cases before wave reflection. For the case of $V_0 = 13.4$ m/s after wave reflection, the strain behind the front increases as the front propagates and the strain in the rod does not reach the densification strain, but for the case of $V_0 = 50.0$ m/s after wave reflection, the reflected wave leads the strain behind the shock front to reach the densification strain. For the case of $V_0 = 109.2$ m/s, a shock front with the densification strain behind it propagates from the proximal end to the distal end and the foam deforms in the *Shock Mode*. Except for the last case, the behaviour of the predictions by the R-P-P-L model is very different from those described above. For any case of impact velocities, the part behind the front is always regarded as being in a locked state by the R-P-P-L model, see Fig. 10a. This assumption is not reasonable when the impact velocity is less than the second critical impact velocity. In this paper, the Transitional-Mode model allows the strain behind the front to be less than the densification strain, which seems more reasonable at a moderate impact velocity. Nevertheless, it needs to be further confirmed by the experimental observations, which is not available because the limits of 3D experimental conditions make it difficult to observe the full deformation process or obtain the distribution of strain in a real specimen.

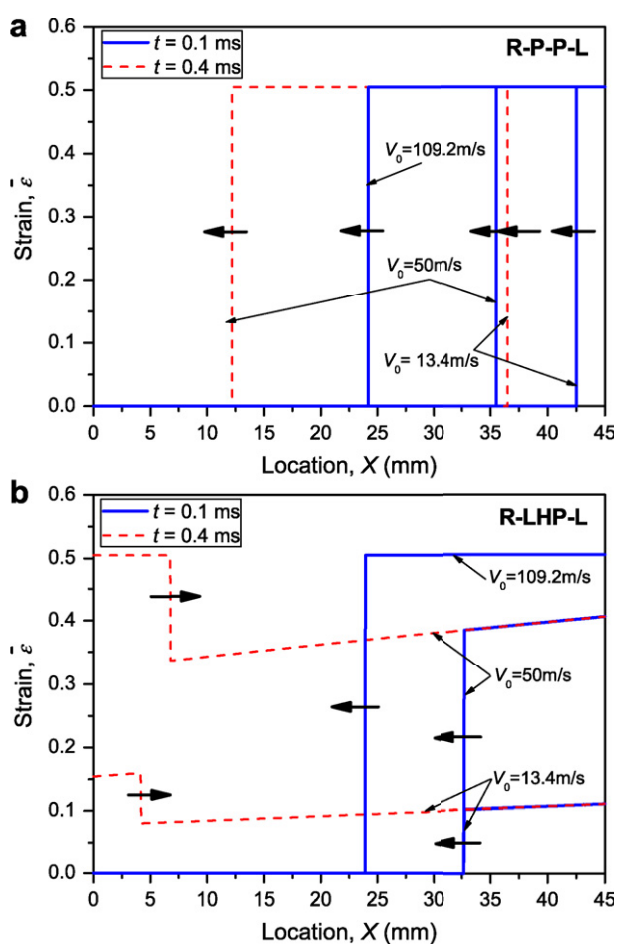

Fig. 10. Strain distributions in the foam rod modelled as (a) the R-P-P-L idealisation and (b) the R-LHP-L idealisation.

5. Conclusions

A *Transitional Mode* has been found numerically and experimentally among the extensive experimental and modelling studies of the dynamic crushing of 2D (honeycomb) and 3D (foam) cellular materials when the impact velocity is not very high. The plateau stress zone in a representative quasi-static stress-strain curve of cellular metals is usually taken as a long ramp in which the strain does not reach the densification strain. However, when the impact velocity is high enough, a *Shock Mode* occurs. In this case, the enhancement of the stress over the quasi-static plateau stress of the specimens no longer depends on the plateau stress.

To illustrate the predicted response of the material, we introduce a rigid–linearly hardening plastic–rigid idealisation of the cellular material to develop both a Transitional-Mode model and a Shock-Mode model. The 'rigid unloading' assumption was employed in the analysis using a one-dimensional continuum-based stress wave theory.

The Shock-Mode model in this paper is essentially the same as the R-P-P-L model [3]. Compatibility conditions at the deformation front and the equation of motion of the striking mass were used to determine the governing equations in our Shock-Mode model. The governing equations are consistent with those derived from the thermo-mechanical approach by Tan et al. [3]. A *Shock Mode* occurs when the initial stress on the impact interface is greater than the densification stress, so a critical impact velocity was expected and presented in this paper. When the impact velocity is less than this critical velocity, the *Shock Mode* will not occur. Moreover, the *Shock Mode* will transform to the *Transitional Mode* when the stress at the wave front is attenuated to be less than the initial densification stress, and the corresponding transition time was presented in this paper. The R-P-P-L model is not appropriate for crushing at low impact velocities. In this paper, as a supplement, the Transition-Mode model with nonzero E_1 has been developed for the crushing with moderate impact velocities.

Two impact scenarios, namely *the rod-target impact* and *the striker-rod impact*, were investigated. The effects of finite striker mass and impact velocity were studied. Inelastic reflected waves were also considered. In our theoretical models, the distributions of stress, strain and velocity in the foam rod were obtained. The theoretical results show that for a *Shock Mode*, behind the front the *initial* strain remains constant and the initial stress varies proportionally with the *square* of the impact velocity, but for a *Transition Mode*, the *initial* strain and stress behind the front reduce *linearly* with reducing impact velocity. During the crushing process, the strain in the unloading zone decreases along the rod axis in the Transitional-Mode model but is locked at a strain (the locking strain) in the Shock-Mode model. The stress behind the front and the velocity of the mass decreases as the wave propagates in the rod. Two dimensionless parameters, namely the shock-enhancement parameter and the *stress-hardening* parameter, were defined. For the striker-rod impact scenario with an infinite rod length, the features of the theoretical predictions were presented.

Compared to the experimental results, the responses at the ends of foam rod, such as the load at the proximal end and the velocity of the distal end, are well predicted by the present models and also by the R-P-P-L model. However, deformation mechanisms uncovered by the present models and the R-P-P-L model are very different when the impact velocity is not very high.

Although the problem of the dynamic crushing of cellular materials is very complicated, the one-dimensional stress wave theory reveals some inherent mechanisms of the dynamic responses that explain some interesting phenomena.

Acknowledgements

This work is supported by the National Natural Science Foundation of China (Projects Nos. 90916026, 11002140 and 90205003), the China Postdoctoral Science Foundation (Project No. 20100470860) and the Chinese Academy of Sciences (Grant No. KJCX2-EW-L03). The authors wish to express their appreciation to Dr. P.J. Tan and Dr. J.J. Harrigan for useful and helpful communications, and to Professor T.X. Yu for facilitating their collaboration on this work.

Appendix

Some basic equations for the rod-target impact scenario are derived here. Similarly, one can obtain those for the striker-rod impact scenario.

Firstly, we consider the rigid mass together with the portion of foam between the mass and the plastic front at time t as a system, see Fig. A.1. This system has a constant value of total mass $M_b+\rho_0A_0L_1$, where $L_1=\Phi(t)$ with $\Phi(t)$ being the location of the front. At time t, the Lagrangian velocity of the front is $\dot{\Phi}(t)$. At time $t+\Delta t$, the front reaches the location $\Phi(t+\Delta t)$ and its Lagrangian velocity is $\dot{\Phi}(t+\Delta t)$, see Fig. A.1. At this time, the foam behind the front changes its velocity from v_b to 0. The external force acting on this system from the right side is $-P_{\text{right}}$, where we take P_{right} as positive in compression. Hence, the condition of momentum conservation of this system can be written as

$$-\int_t^{t+\Delta t} P_{\text{right}}(\tau)\mathrm{d}\tau=(M_b+\rho_0A_0\Phi(t+\Delta t))(v_b(t+\Delta t)-v_b(t)) +\rho_0A_0(-\Delta\Phi)(0-v_b(t)), \tag{A.1}$$

where $\Delta\Phi=\Phi(t+\Delta t)-\Phi(t)<0$. The above equation is equivalent to that by analysing a variable mass system, which is composed by the rigid mass and the portion of foam ahead of the front at any time. It should be noted that selecting the right external force is crucial in the analysis. Dividing Δt on both sides of Eq. (A.1), we obtain

$$-\frac{1}{\Delta t}\int_t^{t+\Delta t} P_{\text{right}}(\tau)\mathrm{d}\tau=(M_b+\rho_0A_0\Phi(t+\Delta t))\cdot\frac{v_b(t+\Delta t)-v_b(t)}{\Delta t} +\rho_0A_0\frac{\Delta\Phi}{\Delta t}v_b(t). \tag{A.2}$$

When $\Delta t\to 0$, the above equation leads to

$$-P_{\text{right}}(t) = (M_b+\rho_0A_0\Phi(t))a_b(t)+\rho_0A_0\dot{\Phi}(t)v_b(t). \tag{A.3}$$

By denoting $M(t)=M_b+\rho_0A_0\Phi(t)$, Eq. (A.3) can also be written as

$$-P_{\text{right}}(t) = \frac{\mathrm{d}}{\mathrm{d}t}(M(t)v_b(t)), \tag{A.4}$$

which corresponds to the classical equation of the Newton's 2nd law for a varying mass problem.

Secondly, we consider the portion of foam between $\Phi(t+\Delta t)$ and $\Phi(t)$ as a system, see Fig. A.2. The external forces acting on this system from the left and right sides are $-P_{\text{left}}$ and $-P_{\text{right}}$, respectively. This system has a velocity of $v_b(t)$ at time t but of 0 at time $t+\Delta t$. Hence, the conservation conditions of mass and momentum of this system can be written as

$$0=\rho_0A_0\left(\int_t^{t+\Delta t}(v_b(\tau))\mathrm{d}\tau-0\right)+\rho_0A_0\left(\int_t^{t+\Delta t}\dot{\Phi}(\tau)\varepsilon_f(\tau)\mathrm{d}\tau-0\right) \tag{A.5}$$

and

$$-\int_t^{t+\Delta t}P_{\text{right}}(\tau)\mathrm{d}\tau+\int_t^{t+\Delta t}P_{\text{left}}(\tau)\mathrm{d}\tau=\rho_0A_0(-\Delta\Phi)(0-v_b(t)), \tag{A.6}$$

respectively. By dividing Δt on both sides and taking the limit as $\Delta t\to 0$, Eq. (A.5) leads to Eq. (3), while Eq. (A.6) can be rewritten as

$$P_{\text{right}}(t)-P_{\text{left}}(t) = \rho_0A_0\dot{\Phi}(t)(0-v_b(t)). \tag{A.7}$$

Putting $P_{\text{left}}=\sigma_0A_0$ and $P_{\text{right}}=\sigma_fA_0$ in the above equation, one can obtain Eq. (4).

Finally, associating Eq. (A.3) with Eq. (A.7) leads to

$$-P_{\text{left}}(t) = (M_b+\rho_0A_0\Phi(t))a_b(t), \tag{A.8}$$

which results in Eq. (1) since $P_{\text{left}}=\sigma_0A_0$.

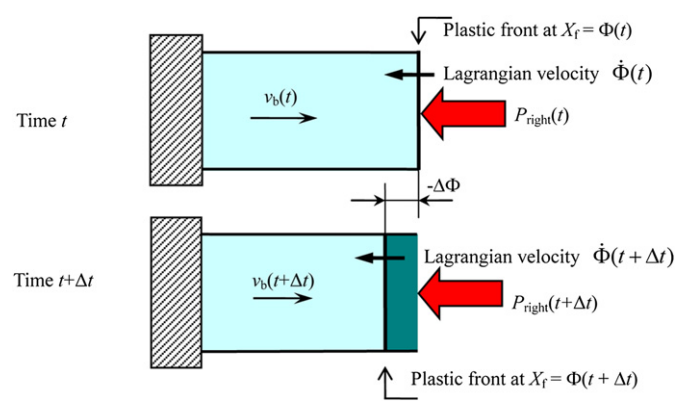

Fig. A.1. Schematic diagram for the system of the rigid mass together with the portion of foam between the mass and the plastic front at time t.

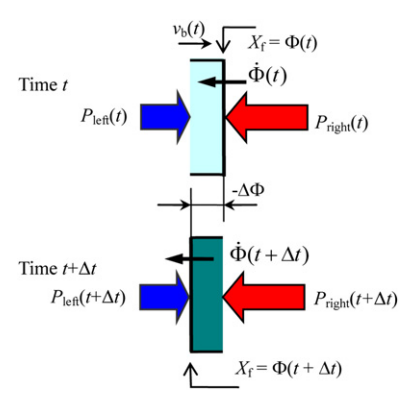

Fig. A.2. Schematic diagram for the system of the portion of foam between $\Phi(t+\Delta t)$ and $\Phi(t)$.

References

[1] Reid SR, Peng C. Dynamic uniaxial crushing of wood. Int J Impact Eng 1997; 19(5–6):531–70.
[2] Tan PJ, Reid SR, Harrigan JJ, Zou Z, Li S. Dynamic compressive strength properties of aluminium foams. Part I — experimental data and observations. J Mech Phys Solids 2005;53(10):2174–205.
[3] Tan PJ, Reid SR, Harrigan JJ, Zou Z, Li S. Dynamic compressive strength properties of aluminium foams. Part II — 'shock' theory and comparison with experimental data and numerical models. J Mech Phys Solids 2005;53(10): 2206–30.
[4] Ruan D, Lu G, Wang B, Yu TX. In-plane dynamic crushing of honeycombs — a finite element study. Int J Impact Eng 2003;28(2):161–82.
[5] Zheng ZJ, Yu JL, Li JR. Dynamic crushing of 2D cellular structures: a finite element study. Int J Impact Eng 2005;32(1–4):650–64.
[6] Liu YD, Yu JL, Zheng ZJ, Li JR. A numerical study on the rate sensitivity of cellular metals. Int J Solids Struct 2009;46(22–23):3988–98.
[7] Zou Z, Reid SR, Tan PJ, Li S, Harrigan JJ. Dynamic crushing of honeycombs and features of shock fronts. Int J Impact Eng 2009;36(1):165–76.
[8] Ma GW, Ye ZQ, Shao ZS. Modeling loading rate effect on crushing stress of metallic cellular materials. Int J Impact Eng 2009;36(6):775–82.
[9] Elnasri I, Pattofatto S, Zhao H, Tsitsiris H, Hild F, Girard Y. Shock enhancement of cellular structures under impact loading: part I experiments. J Mech Phys Solids 2007;55(12):2652–71.
[10] Harrigan JJ, Reid SR, Peng C. Inertia effects in impact energy absorbing materials and structures. Int J Impact Eng 1999;22(9–10):955–79.
[11] Hönig A, Stronge WJ. In-plane dynamic crushing of honeycomb. Part I: crush band initiation and wave trapping. Int J Mech Sci 2002;44(8):1665–96.
[12] Tan PJ. Dynamic mechanical properties of metal foams. PhD thesis. The University of Manchester, U.K., 2005.
[13] Reid SR, Bell WW, Barr RA. Structural plastic shock model for one-dimensional ring system. Int J Impact Eng 1983;1(2):175–91.
[14] Shim VP, Tay BY, Stronge WJ. Dynamic crushing of strain-softening cellular structures — a one-dimensional analysis. ASME J Eng Mat Tech 1990;112(4): 398–405.
[15] Li QM, Meng H. Attenuation or enhancement — a one-dimensional analysis on shock transmission in the solid phase of cellular material. Int J Impact Eng 2002;27(10):1049–65.
[16] Harrigan JJ, Reid SR, Yaghoubi AS. The correct analysis of shocks in a cellular material. Int J Impact Eng 2010;37(8):918–27.
[17] Lopatnikov SL, Gama BA, Haque MJ, Krauthauser C, Gillespie JW. High-velocity plate impact of metal foams. Int J Impact Eng 2004;30(4):421–45.
[18] Li QM, Reid SR. About one-dimensional shock propagation in a cellular material. Int J Impact Eng 2006;32(11):1898–906.
[19] Harrigan JJ, Reid SR, Tan PJ, Reddy TY. High rate crushing of wood along the grain. Int J Mech Sci 2005;47(4–5):521–44.
[20] Pattofatto S, Elnasri I, Zhao H, Tsitsiris H, Hild F, Girard Y. Shock enhancement of cellular structures under impact loading: part II analysis. J Mech Phys Solids 2007;55(12):2671–86.
[21] Miltz J, Ramon O. Energy absorption characteristics of polymeric foams used as cushioning materials. Polym Eng Sci 1990;30(2):129–33.
[22] Avalle M, Belingardi G, Montanini R. Characterisation of polymeric structural foams under compressive impact loading by means of energy-absorption diagram. Int J Impact Eng 2001;25:455–72.
[23] Wang LL. Foundations of stress waves. Amsterdam: Elsevier Science Ltd; 2007. pp. 35–42.
[24] Li K, Gao XL, Wang J. Dynamic crushing behavior of honeycomb structures with irregular cell shapes and non-uniform cell wall thickness. Int J Solids Struct 2007;44(14–15):5003–26.
[25] Yu JL, Zheng ZJ. Dynamic crushing of 2D cellular metals: Microstructure effects and rate-sensitivity mechanisms. Acta Mech Solida Sin 2010;23(S):45–55.